A PbS nanocrystal-C_{60} photovoltaic device for infrared light harvesting

D. M. N. M. Dissanayake,[a] Ross A. Hatton, Thierry Lutz, Cristina E. Giusca, Richard J. Curry, and S. R. P. Silva
Nano-Electronic Centre, Advanced Technology Institute, University of Surrey, Guildford, Surrey GU2 7XH, United Kindom

(Received 24 May 2007; accepted 7 September 2007; published online 26 September 2007)

PbS nanocrystal (nc-PbS)-C_{60} photovoltaic devices are demonstrated, in which nc-PbS function as electron donors, showing infrared photosensitivity up to 1600 nm. Annealing nc-PbS is proved to remove capping oleic acid ligands, studied using x-ray photoelectron spectroscopy, significantly improving the short circuit current, open circuit voltage, and fill factor. The device performance is rationalized by quantum confinement in nc-PbS and energy level alignment at the heterojunction based on direct measurements of nc-PbS ionization potential using ultraviolet photoelectron spectroscopy. © *2007 American Institute of Physics*. [DOI: 10.1063/1.2790730]

Organic photovoltaics (OPVs) have strong potential as a source of low-cost renewable energy.[1] Toward this goal, promising results have been shown by OPVs based on conjugated organic molecules[2,3] and polymers.[4,5] Nanocrystals of inorganic semiconductors exhibit size tunable bandgaps due to quantum confinement effects and can be combined with organic materials to enhance the light harvesting capability of OPVs.[6–9] However, semiconductor nanocrystals can only be processed from solution if capped with organic ligands to render them soluble in common organic solvents, which are detrimental to device operation.[10,11] To harness near infrared wavelengths, which comprise a considerable proportion of the solar spectrum, low bandgap nanocrystals such as PbSe and PbS can be incorporated into OPVs.[12,13] To date, nc-PbS have only been employed as the electron acceptor in hybrid nanocrystal-organic OPVs without direct measurement of the electronic structure of nc-PbS to guide device design and understanding toward realizing their full potential. This letter reports a discrete heterojunction (nc-PbS)-C_{60} hybrid solar device with infrared sensitivity. The nanocrystal layer functions as an electron donor and the device shows quantum efficiencies across the solar spectrum up to 1600 nm. Device performance is rationalized in terms of quantum size effect in nc-PbS and by the interfacial energy level alignment at the heterojunction, as inferred from a direct measurement of the ionization potential of nc-PbS using ultraviolet photoelectron spectroscopy (UPS).

Nc-PbS were synthesized with a narrow size distribution according to a method reported by Hines and Scholes [Fig. 1(a)].[14] Experimental details of material/device synthesis and characterization are given in the accompanying supplementary information.[15] Figure 1(b) shows optical absorption of different size nc-PbS samples analyzed in this paper. Thermogravimetric analysis of as synthesized nc-PbS, given in Fig. 1(c), shows that a weight reduction of 1% occurs in nc-PbS between 100 and 250 °C which can be attributed to the loss of solvent and physorbed oleic acid in the sample. Following this, a dramatic reduction of weight is observed within the 250–500 °C temperature range. We attribute this reduction to pyrolysis of the oleic acid ligands. Further, we note that the weight reduction at 500 °C (23%) correlates with an estimate of the maximum weight percent of oleic acid ligands attached to a single nanocrystal of 5 nm diameter (29%). X-ray photoelectron spectroscopy (XPS) analysis of nc-PbS indicated a reduction in carbon from 41.7% to 22.9% and a reduction in oxygen from 14.3% to 2.0% after annealing under ultrahigh vacuum (UHV) for 1 h at 300 °C. The reduction of oxygen and carbon content after annealing is attributed to the removal of oleic ligands ($CH_3[CH2]_7CH{=}CH[CH_2]_7COOH$). Further evidence of the annealing effect on the capping ligands can be inferred from the XPS spectra shown by Fig. 1(d), which show a shift in the binding energy of $Pb_{4f7/2}$ and $Pb_{4f5/2}$ after annealing at 300 °C under UHV. The $Pb_{4f7/2}$ peak shifts from 138.3 to 136.8 eV subsequently forming a shoulder peak at 137.7 eV, identified by the circle in Fig. 1(d). The $Pb_{4f7/2}$ peak of nc-PbS before annealing in Fig. 1(d) is comparable to the PbO peak binding energy values reported in the literature (138.5 eV),[16,17] and is attributed to Pb bonded to oleic

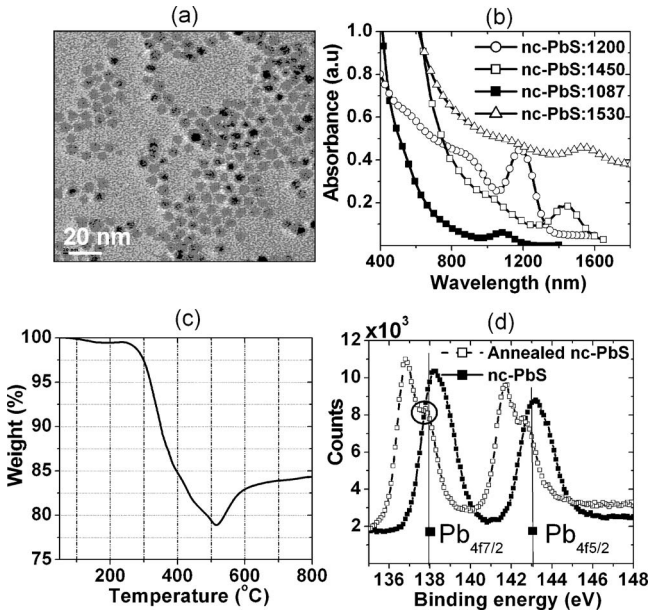

FIG. 1. (a) Transmission electron micrograph of 1450 nm primary absorbing nc-PbS (nc-PbS:1450). (b) Absorbance of oleic acid capped nc-PbS nanocrystals in chloroform. (c) Thermogravimetric analysis of dry nc-PbS annealed under a N_2 atmosphere. (d) XPS spectra of $Pb_{4f7/2}$ and $Pb_{4f5/2}$ in nc-PbS before and after annealing at 300 °C in UHV.

[a]Electronic mail: m.dissanayake@surrey.ac.uk

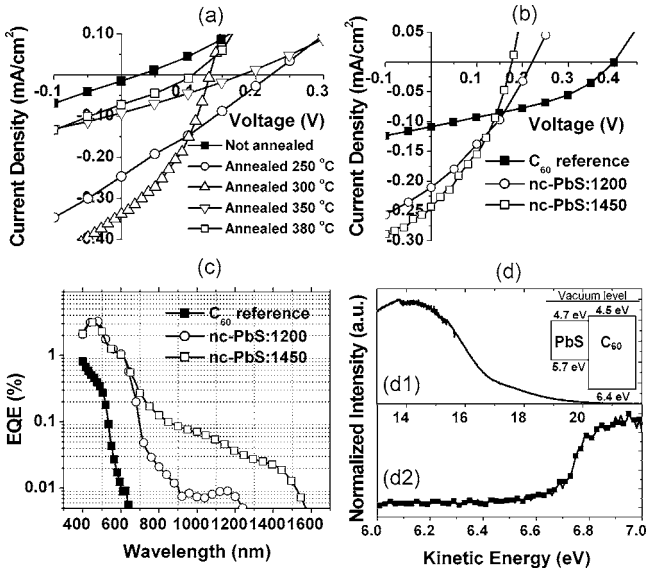

FIG. 2. (a) *J-V* characteristics of ITO/nc-PbS/C_{60} (50 nm)/Al (50 nm) devices measured under AM1.5D, fabricated using nc-Pbs without annealing (black squares), nc-Pbs annealed at 250 °C (circles), nc-PbS annealed at 300 °C (triangles), nc-PbS annealed at 350 °C (deltas), and nc-PbS annealed at 380 °C (white squares). (b) *J-V* plots taken under AM1.5D and (c) external quantum efficiency measurements of ITO/nc-PbS:1200/C_{60} (50 nm)/Al (white circles), ITO/nc-PbS:1450/C_{60} (50 nm)/Al (white squares), and ITO/C_{60} (50 nm)/Al (black squares), respectively. (d) UPS of a nc-PbS sample annealed at 300 °C for 1 h in UHV where (d1) shows the high energy cutoff used to calculate the ionization potential and (d2) shows the low energy cutoff which gives the work function. The inset in (d1) show the proposed flatband energy level diagram for this device.

acid via the —COOH moiety.[18] Similarly, the $Pb_{4f7/2}$ peak value 136.8 eV measured in the annealed nc-PbS sample is in excellent agreement with the reported binding energy for $Pb_{4f/2}$ in PbS.[19] From this evidence, it can be concluded that annealing of the nc-PbS sample resulted in removal of the capping oleic acid ligands from the nanocrystals. However, the removal of the capping ligands also results in the formation of elemental Pb as indicated by the 137.7 eV shoulder peak in the annealed nc-PbS sample shown in Fig. 1(d). The ~3% increase in weight observed after 500 °C in Fig. 1(c) can also be attributed to formation of compounds between elemental Pb and the possible contaminates present in the N_2 flow used during the experiment. Consequently, a compromise must be reached between maximizing ligand removal and minimizing metallic Pb formation. This was empirically determined by utilizing hybrid solar devices, fabricated with nc-PbS layers and annealed at different temperatures, as shown in Fig. 2(a).

Hybrid devices comprising indium tin oxide (ITO)/nc-PbS (140 nm)/C_{60} (50 nm)/Al (50 nm) were fabricated using nc-PbS with a primary absorption at 1200 nm (nc-PbS:1200), annealed at different temperatures. Figure 2(a) shows the current density–voltage (*J-V*) characteristics of these devices from which it is evident that the devices utilizing nc-PbS without annealing exhibit a very small short circuit current density (J_{sc}) of 11 μA cm^{-2}. J_{sc} increases up to 340 μA cm^{-2} when the nc-PbS layer is annealed up to 300 °C. In conjunction with the increase in J_{sc}, the device series resistance (R_s) is decreased, which is evident from the increase in the gradient of the *J-V* characteristic close to open circuit voltage (V_{oc}). The increase in J_{sc} and decrease in R_s can be attributed to pyrolysis of the capping ligands from the nc-PbS, as discussed above. It is expected that the efficiency of exciton dissociation at the heterojunction strongly depends on the distance of separation between donor and acceptor species. The increase in J_{sc} upon removal of the oleic acid ligands is consistent with this expectation. Furthermore, since the oleic acid ligands are intrinsically insulating and the ligand length [2 nm (Ref. 20)] is greater than the charge tunneling barrier, their removal facilitates free carrier transport between adjacent nc-PbS which is consistent with a report by Zhang *et al.*[11] Hence, enhanced charge separation and transport within the active layers after thermal annealing increases the J_{sc} and reduces the R_s, improving the overall performance of the nc-PbS-C_{60} hybrid device. The J_{sc} of the devices is seen to decrease as the annealing temperature is increased above 300 °C. This can be attributed to the formation of elemental Pb on top of the PbS film which quenches excitons formed at the heterojunction. As a result, 300 °C was utilized as the optimum annealing temperature for all devices discussed subsequently in this paper.

As shown in Fig. 2(a), the V_{oc} of devices having a nc-PbS layer subjected to annealing is greater than the device fabricated utilizing the unannealed nc-PbS. The origin of the V_{oc} in heterojunction OPVs is not fully understood,[21,22] although it is widely believed to have a maximum value given by the difference in energy between the donor highest occupied molecular orbital (HOMO) and acceptor lowest unoccupied molecular orbital (LUMO). V_{oc} in OPVs is also known to depend on the alignment between these frontier molecular orbitals and the Fermi level of the adjacent electrode, which can be affected by postdeposition annealing. There are, therefore, two possible explanations for the increase in V_{oc} upon annealing of the nc-PbS layer: It is plausible that the ITO/nc-PbS contact is modified upon removal of the oleic acid ligand, thereby improving alignment between the ITO Fermi level and the relevant transport band in the adjacent nc-PbS. Alternatively, since it is well known that organic adsorbates can affect the work function of inorganic surfaces by modifying the surface potential,[23] it is possible that the offset between the nc-PbS valence band and C_{60} LUMO is reduced in the presence of oleic acid ligands, thereby reducing V_{oc}.

A comparison between the *J-V* characteristics of ITO/nc-PbS (140 nm)/C_{60} (50 nm)/Al (50 nm) devices, fabricated using annealed nc-PbS:1200 and nc-PbS:1450, and the reference ITO/C_{60} (50 nm)/Al device is shown in Fig. 2(b). The nc-PbS:1200-C_{60} and nc-PbS:1450-C_{60} devices show enhanced J_{sc} of 0.21 and 0.24 mA cm^{-2}, respectively, compared to the reference (0.11 mA cm^{-2}). The increased photocurrents in the hybrid devices are attributed to the increased photon harvesting from the solar spectrum by the nc-PbS layer. To confirm this hypothesis and quantify the contribution made by nc-PbS layer to the photocurrent in each device, external quantum efficiency (EQE) measurements were performed. According to the EQE data, given in Fig. 2(c), the reference device shows significant EQE values only up 650 nm, whereas both the hybrid devices show EQE values well into the near infrared region (650–1600 nm). The nc-PbS:1450-C_{60} hybrid device shows an infrared EQE of approximately 0.1% close to 1000 nm and exhibits a significant EQE up to 1600 nm. This confirms the above hypothesis relating to the photon harvesting property of the nc-PbS. The maximum infrared EQE (0.1%) is an order of magnitude lower than the highest EQE of 3.3% for the hybrid devices

obtained at 450 nm which corresponds to the primary absorption region of C_{60}. This reduction can be attributed to the limitation in exciton diffusion in the nanocrystal film and also to the lower absorption coefficient of the nanocrystals (1.4×10^4 cm^{-1} at 1185 nm) relative to the absorption coefficient of C_{60} (1.0×10^5 cm^{-1} at 460 nm).

UPS measurements were carried out to rationalize the thermodynamic feasibility of exciton dissociation at the heterojunction between nc-PbS and C_{60}. Prior to UPS measurements, the nc-PbS sample was annealed at 300 °C under UHV for 1 h. Upon heating, the valence band structures of nc-PbS become visible, with features below 8 eV originating from the *p*-type valence bands of nc-PbS, as well as from the *s*-type bands derived from Pb 6*s* (~8 eV) and S 3*s* (~14 eV), in reasonable agreement with photoemission studies on bulk PbS.[24] Both the work function and the maximum valence band position were determined directly from the He I UPS spectra by fitting straight lines into their low [Fig. 2(d2)] and high kinetic [Fig. 2(d1)] energy cutoffs, respectively, and determining the intersection with the base line of the spectra. By adding the two values, an ionization potential of 5.1 eV was obtained. Using absorption measurements to obtain the energy gap between the first excited electron and hole states (~1 eV), it was possible to calculate the electron affinity (4.7 eV) for nc-PbS:1200.

The proposed flatband structure for the active layers of the hybrid device is given by the inset in Fig. 2(d1). It is clearly energetically favorable for the holes to transfer from the HOMO level of C_{60} (6.4 eV) to the valence band in nc-PbS (5.7 eV). Electrons from the dissociated excitons generated in nc-PbS have to traverse an energy barrier of ~0.2 eV to transfer from the conduction band of the nc-PbS to the LUMO of C_{60}, explaining the low infrared response of the system. As shown in Fig. 2(b), the V_{oc} of nc-PbS:1200-C_{60} and nc-PbS:1450-C_{60}, 0.17 and 0.22 V, respectively, are significantly lower compared to that of the C_{60} reference device (0.39 V). The fill factors of the two hybrid devices nc-PbS:1200-C_{60} and nc-PbS:1450-C_{60} are 0.37 and 0.29, respectively, which are also lower than the fill factor of the reference C_{60} device (0.40) primarily due to the lower shunt resistance. The lower shunt resistance of hybrid devices is thought to be due to the increased susceptibility of the bilayer films to filament formation upon deposition of the electrode. Overall, the reduced fill factor and reduction in V_{oc} results in a lower power conversion efficiency for the hybrid devices, 0.014% (nc-PbS:1200-C_{60}) and 0.015% (nc-PbS:1450-C_{60}), compared to the reference device (0.019%).

In conclusion, (nc-PbS)-C_{60} photovoltaic devices are demonstrated, in which nc-PbS function as electron donors, showing infrared photosensitivity up to 1600 nm. Annealing of the nc-PbS is observed to remove capping oleic acid ligands, studied using XPS, significantly improving the J_{sc}, V_{oc}, and fill factor. Device performance is rationalized in terms of the quantum confinement in nc-PbS and through heterojunction energy level alignment based on direct measurements of the nc-PbS ionization potential using UPS. The devices reported demonstrate the potential for the development of optimized hybrid organic-inorganic photovoltaic devices utilizing the near infrared solar spectrum.

The authors wish to thank the EPSRC for a Portfolio Partnership award and First grant which has facilitated the research conducted in this project and the studentship awarded. The authors also like to thank Dr. Paul Watts, Dr. Simon Henley, Dr. Nick Blanchard, and Dr. Yann Tison.

[1] S. E. Shaheen, D. S. Ginley, and G. E. Jabbour, MRS Bull. **30**, 10 (2005).
[2] P. Peumans and S. R. Forrest, Appl. Phys. Lett. **79**, 126 (2001).
[3] J. G. Xue, S. Uchida, B. P. Rand, and S. R. Forrest, Appl. Phys. Lett. **85**, 5757 (2004).
[4] S. E. Shaheen, C. J. Brabec, N. S. Sariciftci, F. Padinger, T. Fromherz, and J. C. Hummelen, Appl. Phys. Lett. **78**, 841 (2001).
[5] G. Li, V. Shrotriya, J. S. Huang, Y. Yao, T. Moriarty, K. Emery, and Y. Yang, Nat. Mater. **4**, 864 (2005).
[6] N. C. Greenham, X. Peng, and A. P. Alivisatos, Phys. Rev. B **54**, 17628 (1996).
[7] W. U. Huynh, J. J. Dittmer, and A. P. Alivisatos, Science **295**, 2425 (2002).
[8] B. Sun, H. J. Snaith, A. S. Dhoot, S. Westenhoff, and N. C. Greenham, J. Appl. Phys. **97**, 014914 (2005).
[9] H. J. Snaith, G. L. Whiting, B. Sun, N. C. Greenham, W. T. S. Huck, and R. H. Friend, Nano Lett. **5**, 1653 (2005).
[10] E. Arici, H. Hoppe, F. Schäffler, D. Meissner, M. A. Malik, and N. S. Sariciftci, Thin Solid Films **451-452**, 612 (2004).
[11] S. Zhang, P. W. Cyr, S. A. McDonald, G. Konstantatos, and E. H. Sargent, Appl. Phys. Lett. **87**, 233101 (2005).
[12] S. A. Mcdonald, G. Konstantatos, S. Zhang, P. W. Cyr, E. J. D. Klem, L. Levina, and E. H. Sargent, Nat. Mater. **4**, 138-U14 (2005).
[13] A. Maria, P. W. Cyr, E. J. D. Klem, L. Levina, and E. H. Sargent, Appl. Phys. Lett. **87**, 213112 (2005).
[14] M. A. Hines and G. D. Scholes, Adv. Mater. (Weinheim, Ger.) **15**, 1844 (2003).
[15] See EPAPS Document No. E-APPLAB-91-037740 for experimental details of PbS quantum dot synthesis and hybrid photovoltaic device fabrication and characterization. This document can be reached through a direct link in the online article's HTML reference section or via the EPAPS homepage (http://www.aip.org/pubservs/epaps. html).
[16] S. Chen and W. Liu, Mater. Chem. Phys. **98**, 183 (2006).
[17] K. Laajalehto, R. St., C. Smart, J. Ralston, and E. Suoninen, Appl. Surf. Sci. **64**, 29 (1993).
[18] A. Lobo, T. MÖller, M. Nagel, H. Borchert, S. G. Hickey, and H. Weller, J. Phys. Chem. B **109**, 17422 (2005).
[19] X. Changqi, Z. Zhichen, W. Hailong, and Y. Qiang, Mater. Sci. Eng., B **104**, 5 (2003).
[20] D. Qi, M. Fischbein, M. Drndić, and S. Šelmić, Appl. Phys. Lett. **86**, 093103 (2005).
[21] C. J. Brabec, A. Cravino, D. Meissner, N. S. Sariciftci, T. Fromherz, M. T. Rispens, L. Shanchez, and J. C. Hummelen, Adv. Funct. Mater. **11**, 374 (2001).
[22] D. M. N. M. Dissanayake, R. A. Hatton, R. J. Curry, and S. R. P. Silva, Appl. Phys. Lett. **90**, 113505 (2007).
[23] S. Khodabakhsh, S. M. Sanderson, J. Nelson, and T. S. Jones, Adv. Funct. Mater. **16**, 95 (2006).
[24] T. Grandke, L. Ley, and M. Cardona, Phys. Rev. B **18**, 3847 (1978).